Smart Structures and Systems, *Vol. 17, No. 4 (2016) 559-576*
DOI: http://dx.doi.org/10.12989/sss.2016.17.4.559

Structural behavior of precast concrete deck with ribbed loop joints in a composite bridge

Dong-Ho Shin*[1], Chul-Hun Chung[2], Hyun-Chul Oh[1], Se-Jin Park[1], In-Gyu Kim[1], Young-Jin Kim[1], Tae-Kwan Byun[2] and Myoung-Gu Kang[2]

[1]*Daewoo Institute of Construction Technology, 60 songjuk-dong, Jangan-gu, Suwon-si, Gyeonggi-do, Korea*
[2]*Department of Civil Engineering, Dankook University, 152 jukjeon-ro, Suji-gu, Yongin-si, Gyeonggi-do, Korea*

(Received December 19, 2015, Revised February 20, 2016, Accepted February 30, 2016)

Abstract. This study is intended to propose a precast bridge deck system, which has ribbed loop joints between the decks and lacks internal tendons to improve the workability of existing precast deck system. A composite bridge deck specimen was fabricated using the proposed precast deck system, and static and fatigue load tests were conducted to evaluate the structural behavior and the crack pattern of the deck. Leakage test of the deck joints was also conducted and finite element analysis was carried out to compare with the test results.

Keywords: precast bridge deck system; composite bridge deck specimen; static and fatigue load tests; structural behavior; finite element analysis

1. Introduction

Precast concrete deck has the advantage in reducing construction time and improving the quality of concrete. Due to the advantages, precast desks are an effective alternative to cast-in-place concrete decks where quick construction is required such as replacement construction in urban areas. The demand for precast decks are increasing, and related research is continuously increasing. (Issa *et al.* 1995, Chang 1997, Kim 1997, Youn 1998, Chung 1999, Shim 1999)

For precast concrete decks, serviceability such as cracks and leakage in the joint is very critical, and the performance of the structure is dependent on the joint. Thus, a quick and cost efficient joint connection method while securing required strength and serviceability is important. Many studies have been conducted to develop joint connection methods using longitudinal tendon and loop reinforcement. (Shim 2001, Kim 2004, Kim 2007, Ryu 2007)

Among existing joint connection methods, precast deck system using internal longitudinal tendon(see Fig. 1) has been more widely used, which inserts tendons into the concrete deck to achieve continuity between the decks, as shown in Fig. 1. This system has superior structural performance and serviceability; however, the construction cost increases due to the internal tension work of tendons, and the workability is unfavorable due to the high difficulty of construction. Precast deck system using loop reinforcement is cost efficient and has good workability, but

*Corresponding author, Senior researcher, E-mail: dongho.shin@daewooenc.com

http://www.techno-press.org/?journal=sss&subpage=8 ISSN: 1738-1584 (Print), 1738-1991 (Online)

serviceability may be of concern due to high risk of cracks and leakage in the joint from cast-in-place joints between the decks.

The study on precast deck system that meets the requirements in strength, cost efficiency and construction time by improving the shortcomings of existing methods has been continuously carried out. Recently, the study on flexural performance of precast deck system using symmetric ribbed loop joints without internal tendon has been conducted, and the element test was conducted in comparison with jointless RC deck. (Shin *et al.* 2015).

2. Propsal of precast deck system

2.1 Overview

Following the study on precast deck system with symmetric ribbed loop joints (Shin *et al.* 2015), precast deck system with asymmetric ribbed loop joints is proposed (see Fig. 2), and the structural performance and serviceability is evaluated through static and fatigue load tests of a composite bridge deck. The proposed precast deck system is expected to replace deteriorated bridge decks in urban areas or be applied to new construction projects.

Fig. 1 Precast deck system using internal tendon

Fig. 2 Precast deck system with ribbed loop joints

2.2 Proposal of precast deck system with ribbed loop joints

As aforementioned, precast deck system with asymmetric ribbed loop joints using non-shrinkage mortar at the joint without longitudinal tendon is proposed. Fig. 3 shows the proposed precast deck module and system.

Two types of factory-prefabricated precast deck module A and B with loop reinforcement is placed on girders before placing non-shrinkage high strength mortar into the deck joints so as to make the decks continuous. In Figs. 3(a)-3(b), the loop reinforcement of deck module A and B is embedded, and the modules have asymmetric structure with different partition wall lengths. The ribbed type section is applied to enhance the adhesive strength of the joint between the decks. As shown in Fig 3(c), precast deck modules are placed at the site, and high strength non-shrinkage mortar is placed into the joint between the decks without separate forms, which results in rapid construction.

For precast deck modules, partition walls are installed transversely at specific intervals on the extended lower concrete at the joint, and the loop reinforcement is embedded into the lower concrete for strengthening; therefore, the precast deck modules can be protected from damage during transport and installation.

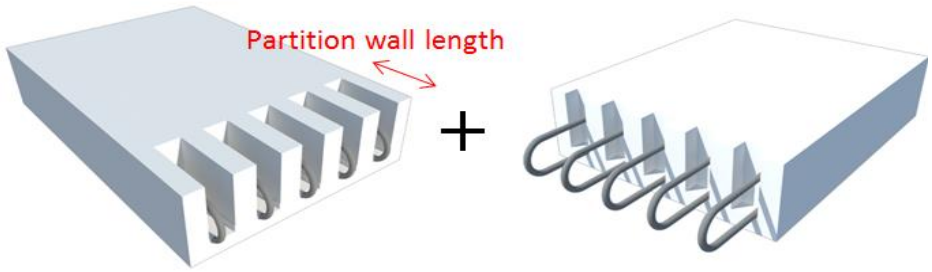

(a) Precast deck module A + Precast deck module B

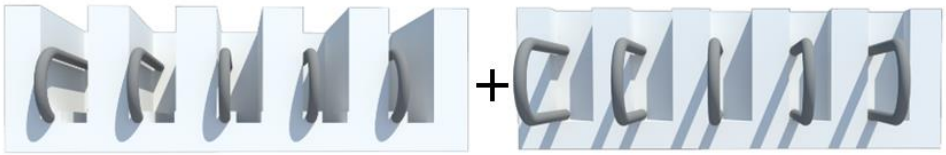

(b) Precast deck module A + Precast deck module B (front view)

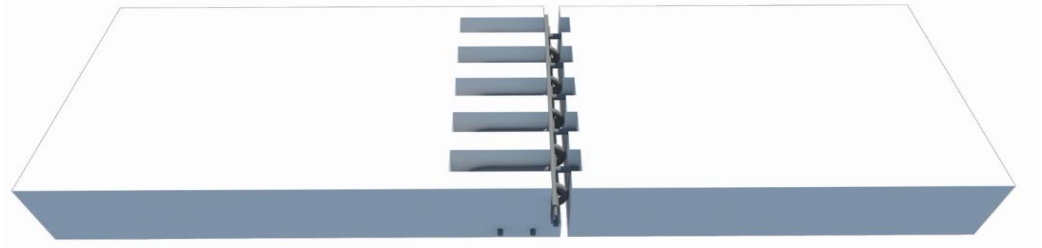

(c) Precast deck system with ribbed loop joints

Fig. 3 Precast deck module and system

2.3 Characteristics of the precast deck system with ribbed loop joints

Fig. 4 shows the details of the precast deck system. Fig. 4(a) shows the details of a typical symmetric precast deck system previously researched while Fig. 4(b) shows the asymmetric precast deck system proposed in this study.

Workability of the symmetric and asymmetric precast deck systems are compared and analyzed in Fig. 5. As shown in Fig. 5, the typical symmetric precast deck system with ribbed loop joints is a horizontally symmetric structure, and sequential vertical installation is impossible because of interference the loop reinforcement extended from the previously installed deck and extended lower concrete of the deck being installed. Furthermore, a separate form is needed when placing non-shrinkage mortar on the sidewall of the joint.

On the contrary, the proposed asymmetric precast deck system lacks interference between the loop reinforcement and extended lower concrete at the joint, allowing sequential vertical installation and good workability. Furthermore, as the partition wall of the joint serves as a form when placing non-shrinkage mortar, a separate form is not required. And, therefore, rapid construction is possible.

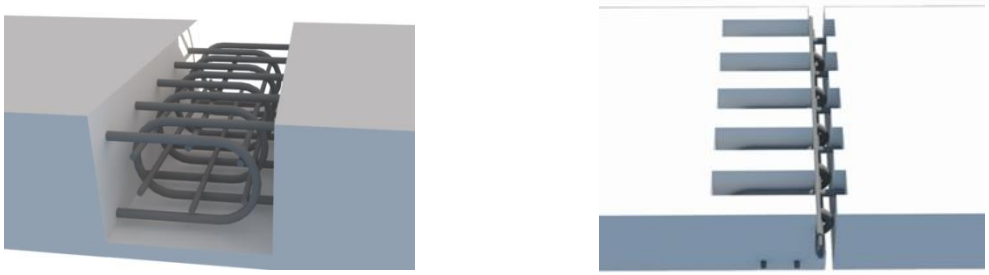

(a) symmetric(previous) (b) asymmetric (Proposed)

Fig. 4 Details of precast deck system

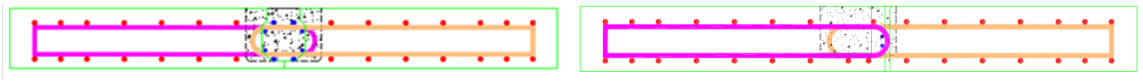

(a) symmetric(previous) (b) asymmetric (Proposed)

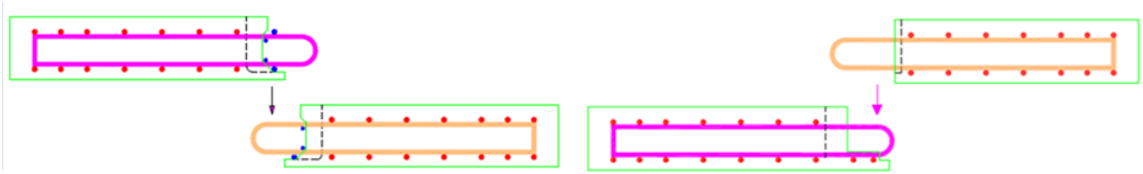

(c) Symmetric allowing no vertical installation (d) Asymmetric allowing vertical installation

Fig. 5 Improved workability by applying asymmetric precast deck system

3. Static and fatigue test on the precast deck of the composite bridge

3.1 Overview

A two-girder composite bridge is fabricated for static and fatigue tests to evaluate the flexural performance of the proposed precast deck system. The mean concrete compressive strength of precast deck specimen is 45 MPa, yield strength of the deformed bar is 400 MPa and the mean compressive strength of the non-shrinkage mortar for deck joint is 55 MPa.

3.2 Composite bridge deck tests

Specification of the composite bridge deck specimen is show in Fig. 6. The specimen of the deck has a width of 4.6 m, length of 10 m, and thickness of 240 mm; furthermore, 19 mm diameter reinforcing bars with spacing on center of 150 mm is used. The girder has a spacing on center of 2.65 m and has a simply support configuration at both ends. After placing two 11.6 m steel girders longitudinally, five precast concrete deck modules are placed on the steel girders, and the non-shrinkage mortar is placed on the deck joint for fabrication of the composite bridge.

To simulate the KL-510 real wheel tread according to the revised design criteria in South Korea, a 231 mm x 577 mm steel plate is placed on the central deck joint boundary as shown in Fig. 6 before applying static load and fatigue load using 2000 kN and 500 kN capacity hydraulic actuators.

In static and fatigue load tests, load is applied on the plate to evaluate the structural behavior and serviceability of the bridge deck, and leakage test is also conducted. For static load test, two times the KL-510 rear wheel load is applied considering the impact coefficient. For fatigue load test, 90 kN including 78 kN of a single rear wheel load from fatigue design and 15% of the design impact load (IM) is applied repeatedly for 2,000,000 cycles to evaluate the fatigue performance. Furthermore, 270 kN, which is 3 times the design fatigue load, is applied repeatedly for 100,000 cycles to investigate the fatigue behavior. Static load is applied until final failure of the deck, and the ultimate performance and failure pattern is evaluated. The test process and load application by stage are summarized in Table 1.

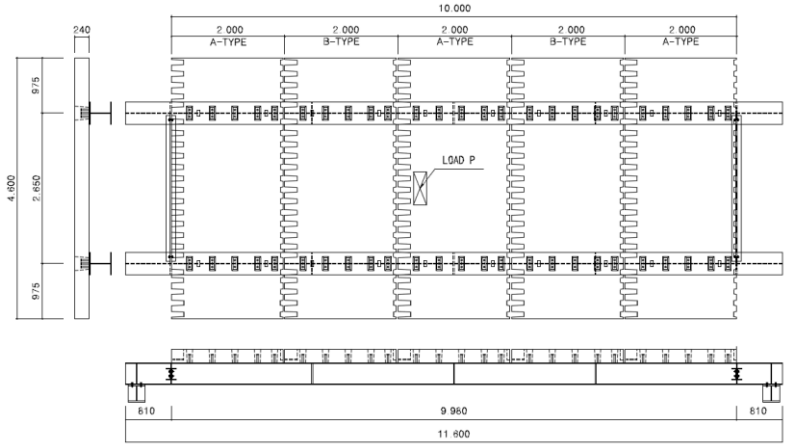

Fig. 6 Specification of composite bridge deck specimen

Table 1 Test process by stage

Stage	Test	Objective	Description	Load (kN)
1	Fatigue test	Fatigue, crack, leakage of deck	- Number of repeated loading cycles : 2,000,000 (Static test at 1,10,100,1000,10000,100000, 1000000 and 2000000) - design fatigue load - No leakage after fatigue test	30~90
2	Static test	Crack behavior of deck	- Single static load - Two times the design load considering impact effect - Initial longitudinal crack in deck occurred (240kN)	0~250
3	Fatigue test	Fatigue, crack, leakage of deck	- Number of repeated loading cycles : 100,000 (Static test at 1,10,100,1000,10000 and 100000) - Additional longitudinal crack in deck occurred and developed - No leakage after fatigue test	30~180, 30~270
4	Static test	Ultimate behavior and failure of deck	- Single static load - Punching shear failure occurred in deck (1146kN)	0~1146

3.3 Measurement

Gauges are installed as shown in Fig. 7 to measure deck deflection, crack width and rebar strain during static and fatigue load test. Six LVDTs are installed at the bottom of the deck, and six crack gauges are installed. Four crack gauges are installed at the bottom of the deck joint before applying the load, and two crack gauges are installed on the occurrence of cracks at the bottom of deck to measure the crack width. Rebar strain gauges are installed inside the precast deck and on the reinforcement at the joint between the decks.

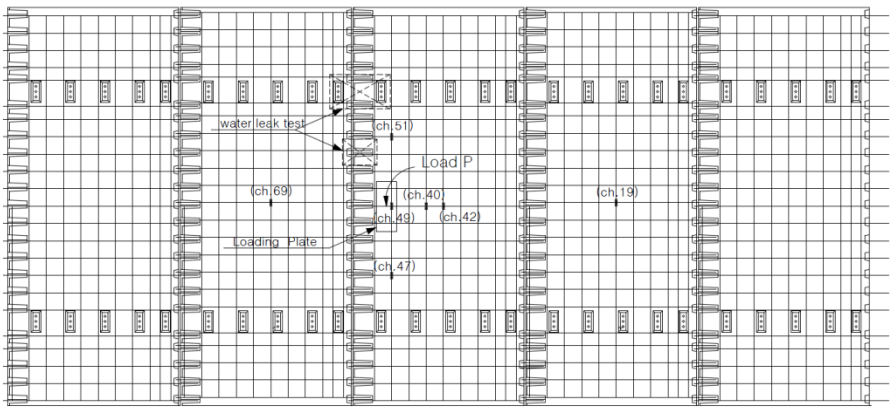

(a) Strain gauge location on the main reinforcement

Continued-

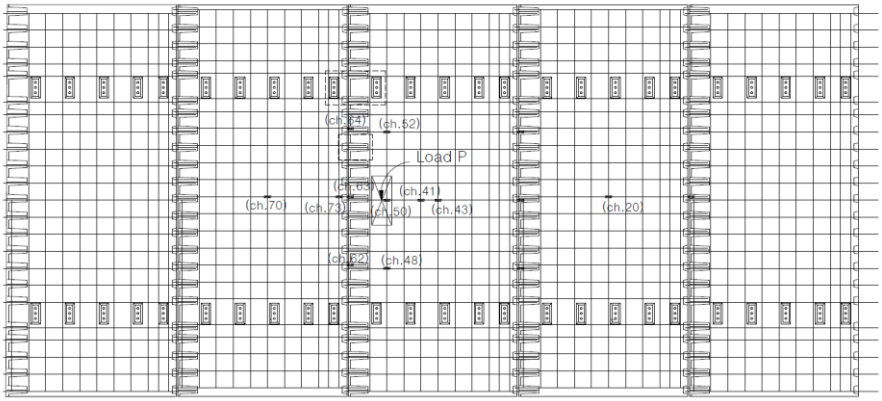

(b) Strain gauge location on the longitudinal reinforcement

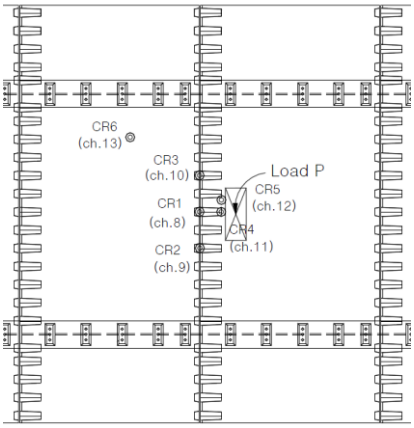

(c) Crack gage

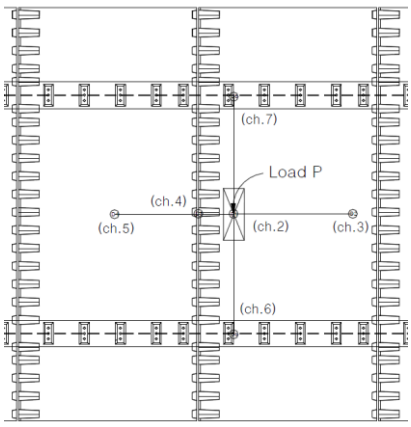

(d) Deflection gauge (LVDT)

Fig. 7 Location of gauges (At the bottom of the deck)

(a) Form fabrication & concrete pouring

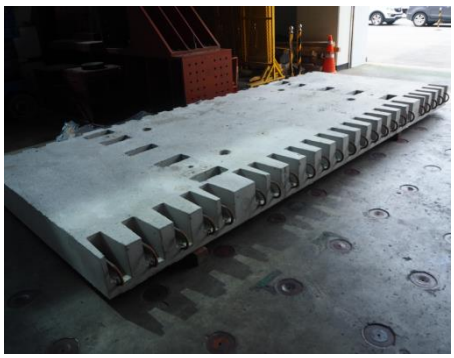

(b) PC deck prefabrication

Continued-

(c) Steel girder & cross beam installation

(d) PC deck installation

(e) Completion of PC deck installation

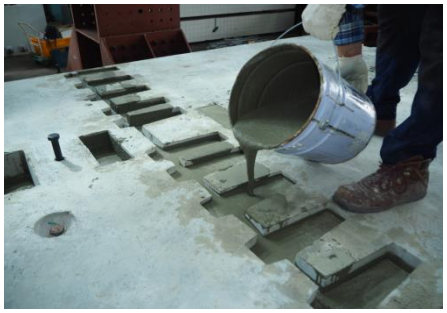

(f) Non-shrinkage mortar into Joint

(g) Gauge installation at the bottom of deck

(h) Load application and leakage test

Fig. 8 Test of the composite bridge deck system

For a composite bridge using precast decks, constraining leakage and cracks in the joint of the decks and at the connection of the deck and steel girder is very important. Thus in this study, load application and leakage test are carried out to check for cracks and leakage under static and fatigue load condition. Leakage test as shown in Fig. 7(a) is conducted in the joint between the decks and at the connection between the steel girders and the decks.

Fig. 8 shows the fabrication of the bridge deck and the test process. After setting the factory-prefabricated steel girders and the precast decks, non-shrinkage mortar is placed into the joint between the decks and the connection between the decks and steel girders of the composite bridge. After setting the gauges on the deck and reinforcement, structural performance and serviceability of the deck are evaluated by applying each load conditions of each stage.

4. Test result evaluation and analysis

4.1 Static test

Load-deflection curve at the four LVDT locations after a single point at the joint boundary on the central deck is shown in Fig. 9(a). The figure shows a linear load-displacement behaviour until the load reaches 400 kN, and thereafter a nonlinear load-displacement behaviour is observed until punching shear occurs at a maximum load of approximately 1,146 kN. Fig. 9(b) shows the ultimate failure at the bottom of the central deck. The punching failure strength of the deck is approximately 9.1 times the design load considering the impact effect, and the failure surface at the bottom is approximately 200 cm x 180 cm.

Fig. 10 shows the crack and failure pattern at the bottom of the deck by each load stage.

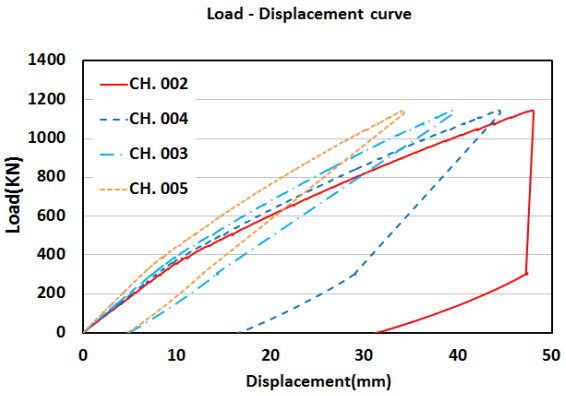

(a) Load-deflection curve

(b) Punching shear failure at the bottom of the deck

Fig. 9 Load-deflection curve and punching shear failure

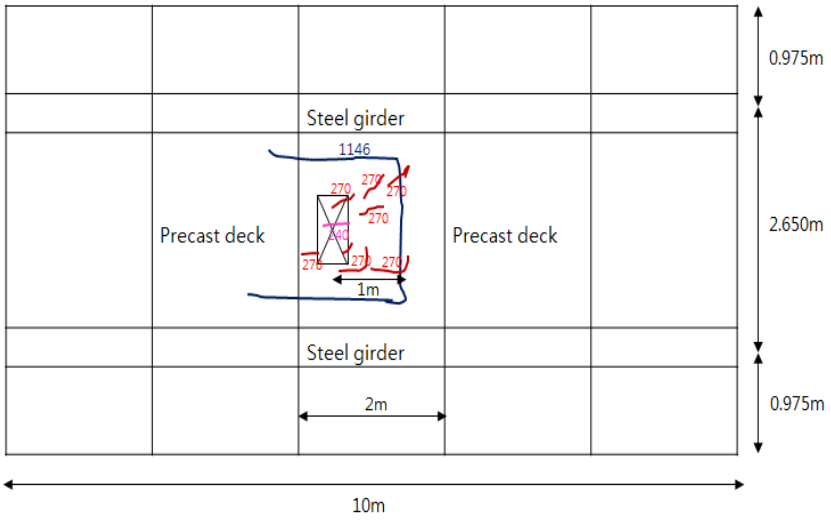

Fig. 10 Crack pattern by the load size of each stage (kN)

As shown in Fig. 10, at stage 1 fatigue load test (maximum load of 90 kN), cracks are not found at the bottom of the deck visually.

Initial longitudinal crack is monitored with visually at the bottom of the loading surface at 240 kN during stage 2 of the static load test (maximum load of 250 kN).

After stage 3 fatigue load test (maximum load of 270 kN), several longitudinal cracks at the bottom of the deck are observed, but lateral cracks and leakage in the joints are not found.

At stage 4 static test (maximum load of 1,146 kN), cracks develop to the left of the loading surface until punching shear failure occurs as indicated with the blue line when the load reaches 1,146 kN. Viewing the crack patterns before ultimate failure, existing longitudinal cracks at the bottom of the central deck extends through the lateral joint between the decks, and the cracks occur to the left of the deck until punching shear failure is reached, as shown in Fig. 10. At ultimate shear failure, punching failure surface mainly occurs to the right of the central deck loading surface. Geometric and material property differences, such as connection details and bond strength of the filling material at the precast deck joint, affect the local stress concentration and local shear strength and thus show unpredictable shear failure behavior. Concerning this ultimate failure pattern, further analysis shall be required.

Fig. 11 shows the load-strain curve of the main reinforcement at the bottom of the deck during stage 4 static load test (maximum load of 1,146 kN). From the figure, the strain of the rebar increases linearly until approximately 300 kN and increases nonlinearly thereafter. The rapid increase of the main rebar strain can be considered by the rise of the neutral axis due to crack occurrence at 240 kN to 300 kN and damage at the bottom of the deck.

Fig. 12 shows the strain of the main and longitudinal reinforcement at the bottom of the deck at stage 4 static load test (maximum load of 1,146 kN). As shown in Fig. 12, the stress of the main reinforcement at the center of the deck is significantly higher than the strain of the longitudinal reinforcement, and thus causing the main reinforcement to bear more load. The load bearing level of the longitudinal reinforcement is relatively higher at the loading surface than the center of the deck.

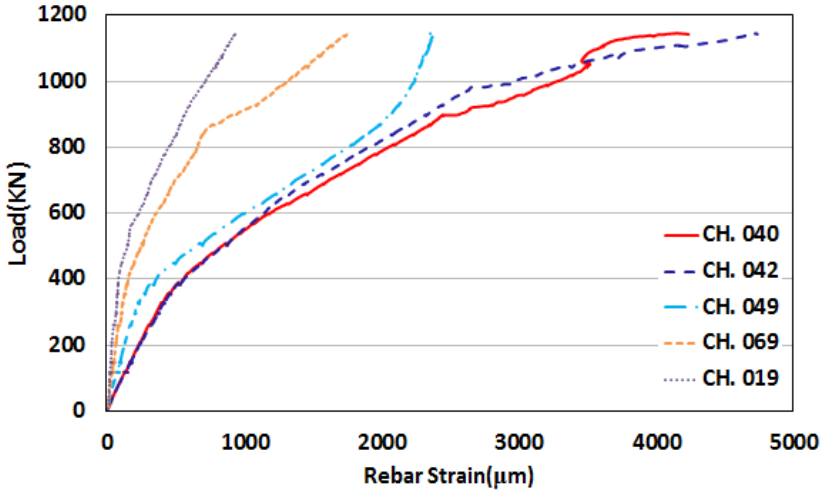

Fig. 11 Load-strain curve of main reinforcement at the bottom

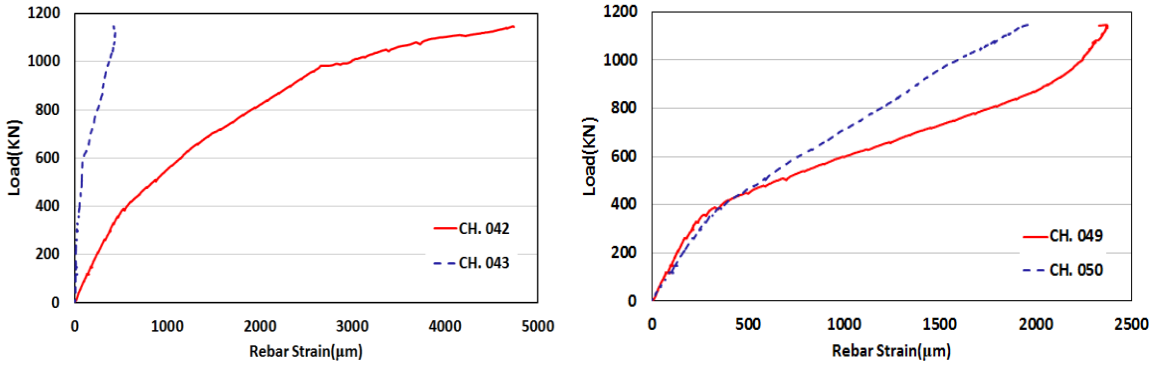

(a) at the Center of the deck (b) at Loading Area

Fig. 12 Load-strain curve of reinforcement at the bottom (main vs longitudinal reinforcement)

4.2 Fatigue test

Static load test is carried out with repeated load cycles at the center deck joint boundary until the completion of stage 1 fatigue load test (maximum load of 90 kN), and the load-displacement measurement results are shown in Fig. 13. Residual defelection increases with the number of load cycles, but the deflection behaves linearly. Cracks and leakage did not occur by visual inpection.

The load-deflection curve at the joint boundary loading surface from repeated fatigue load of 90 kN, 180 kN, 270 kN and static load thereafter is shown in Fig. 14. After completing 100,000 cycles of 180 kN and 270 kN load, the residual deflection increase, and the gradient gradually decrease; furthermore, the stiffness of the deck slightly decrease depending on crack occurrence in the deck but still show linear behavior.

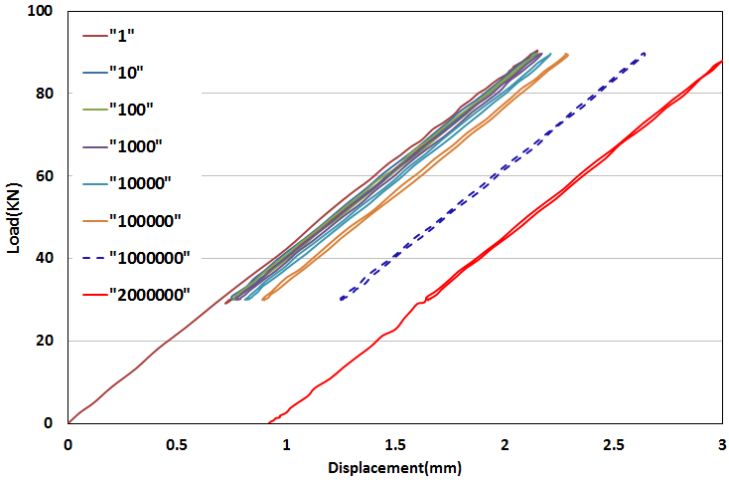

Fig. 13 Load-deflection curve (after stage 1 fatigue load test)

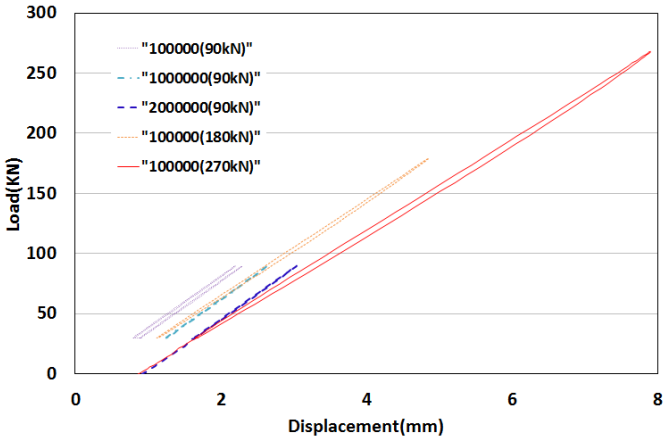

Fig. 14 Load-deflection curve (at the joint boundary loading surface)

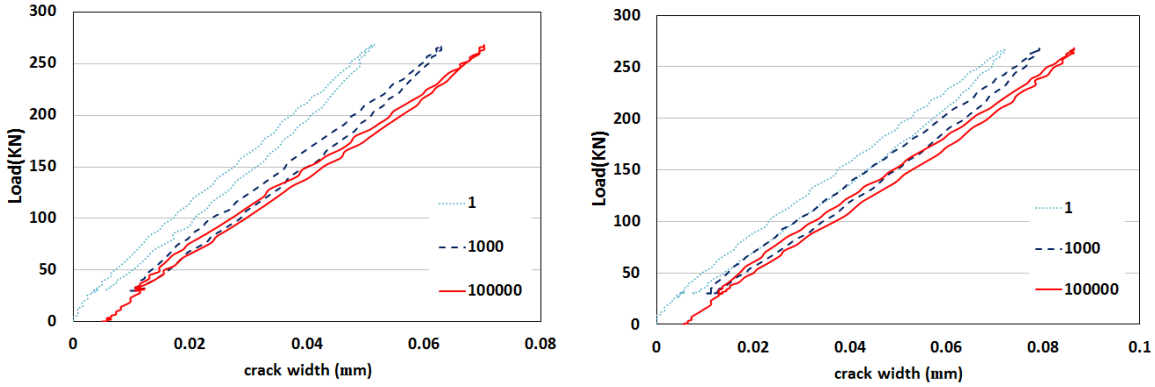

At the bottom of joint between decks (CH.11) (b) Initial crack point (CH.12)

Fig. 15 Load-crack width curve in line with repeated fatigue load(30~270 kN)

Fig. 15 shows the load-crack width curve at the bottom of the joint between the decks (CH.11) and at the initial crack location (CH.12) after applying 100,000 cycles of repeated 270 kN fatigue load on the boundary of the joint at the center of the deck. The crack width measured at the initial stage of the repeated load is less than 0.1 mm, and the crack width increases with the number of load cycles. However, the crack width is within allowable crack width of 0.2 mm, and leakage at the joints and connections doesn't occur; furthermore, lateral cracks don't occur by visual inspection.

5. Finite element analysis of the composite bridge deck specimen

A non-linear finite element analysis of the composite bridge deck specimen is carried out using a finite element analysis program, ABAQUS 6.9(2009). The center two joints are modeled for

finite element analysis even though the specimen has four joints, because tests results show that the loads do not influence the joints at the ends. An 8-node solid element is used for concrete and non-shrinkage mortar. A 2-node 3D Truss element (T3D2) is used for reinforcement, and concrete and reinforcement are assumed to be fully bonded by applying embedded region. Contact condition is considered at the boundary between concrete and non-shrinkage mortar. Finite element model of the specimen is shown in Fig. 16.

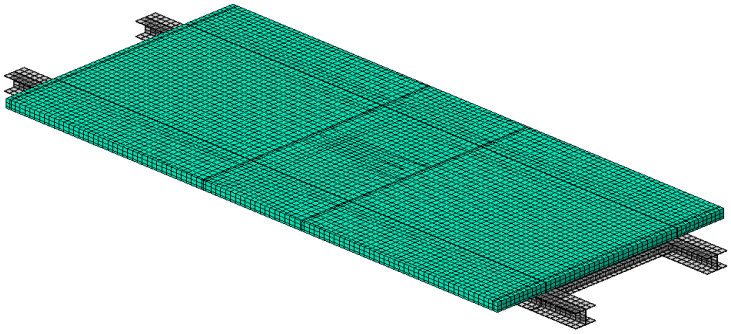

(a) Full model

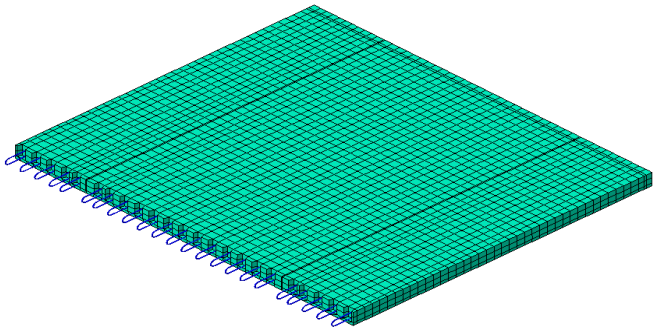

(b) Left side cross section of joint

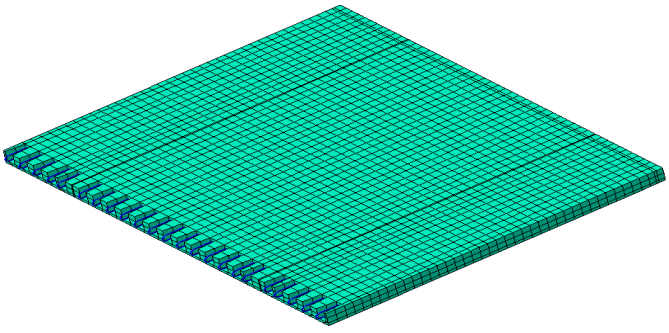

(c) Right side cross section of joint

Fig. 16 Finite element analysis model of the composite bridge model

Table 2 Material properties of concrete

Compressive strength(MPa)	Tensile strength(MPa)	Elastic modulus(MPa)	Mass density(kg/m^3)	Poisson ratio
45	2.25	33,060	2300	0.18

The concrete compressive stress-strain relationship is evaluated using Modified Hognestad stress-strain curve, as shown in Eq. (1) and Fig. 17. Compressive strength of the specimen is used for analysis, and strain ε_o and ultimate strain ε_{cu} are 0.0025 and 0.0035, respectively. Linear elastic section of concrete is assumed 30% of the compressive strength. Tensile strength of concrete is set as 5% of the compressive strength, and the tensile characteristics after crack occurrence is a perfectly plastic model considering tensile stiffening effect and convergence (Song *et al*. 2009). Concrete Damaged Plasticity model is used as the failure standard for the plastic model of concrete. Material characteristics of concrete used for finite element analysis are summarized in Table 2.

$$f_c = f_c'\left[\frac{2\epsilon_c}{\epsilon_o} - \left(\frac{\epsilon_c}{\epsilon_o}\right)^2\right] \qquad 0 < \epsilon_c < \epsilon_t \tag{1a}$$

$$f_c = f_c'\left[1 - 0.15\left(\frac{\epsilon_c - \epsilon_o}{\epsilon_{cu} - \epsilon_o}\right)\right] \qquad \epsilon_o < \epsilon_c < \epsilon_{cu} \tag{1b}$$

The compressive strength of non-shrinkage mortar used in the specimen, 55MPa, is applied for analysis, and Concrete Damaged Plasticity model is used. Material characteristics of non-shrinkage mortar are based on data in previous studies. That is, perfectly elasto- plastic model is used; the linear elastic section of concrete is assumed 30% of the compressive strength, and the tensile strength is set as 1.10MPa or 2% of the compressive strength (Joo *et al*. 2014). Strain ε_o and ultimate strain ε_{cu} are 0.013 and 0.017, respectively, and the elastic modulus is set as 11,000 MPa according to Eq. (2) (Kaushik *et al*. 2007). Stress-strain relationship of non-shrinkage mortar used for finite element analysis is shown in Fig. 18.

$$E_m = 200 f_m' \tag{2}$$

Where, f'm : Unconfined compressive strength of non-shrinkage mortar (MPa).

Yield strength of reinforcement used for the specimen is 400MPa, and the material is assumed a perfect elastic model, as shown in Fig. 19, and reinforcement and concrete are assumed to be completely bonded by applying embedded region condition.

Yield strength of reinforcement used for the specimen is 400 MPa, and the material is assumed a perfect elastic model, as shown in Fig. 19, and reinforcement and concrete are assumed to be completely bonded by applying embedded region condition.

Material characteristics of reinforcement used for the analysis are summarized in Table 3.

Table 3 Reinforcement material properties

Yield strength(MPa)	Elastic modulus(MPa)	Mass density(kg/m^3)	Poisson ratio
400	20,000	7,850	0.3

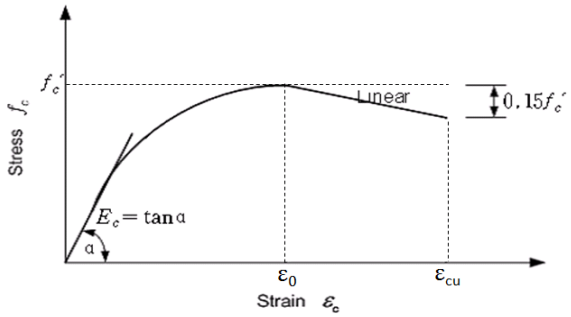

Fig. 17 Modified Hognestad stress-strain curve of concrete (Hognestad 1951)

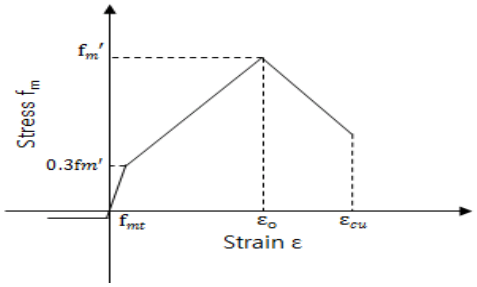

Fig. 18 Stress-strain relationship of non-shrinkage mortar

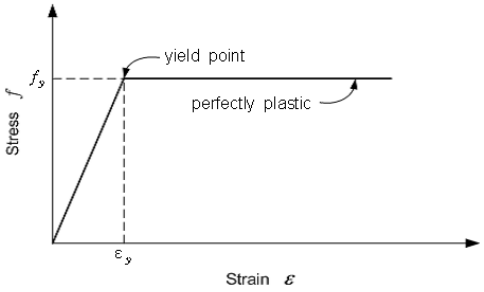

Fig. 19 Stress-strain relationship of rebar

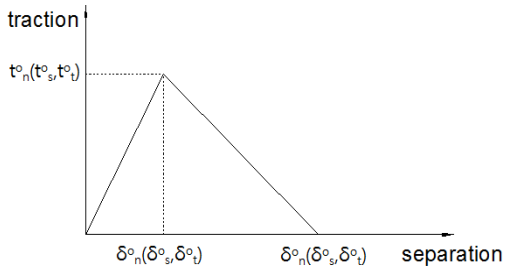

Fig. 20 Relationship between bond strength and bond failure

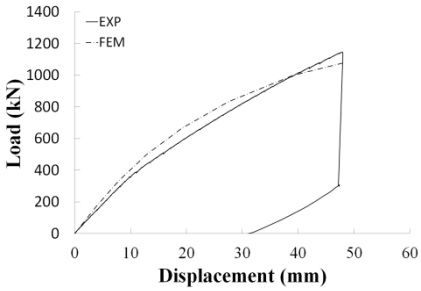

Fig. 21 Comparison of load-displacement between experiment and analysis

In this analysis, contact condition is applied to the joint boundary between concrete and non-shrinkage mortar to enable occurrence of perpendicular openings to the boundary surface. The applying bond stress increases linearly until the bond strength of the boundary surface in the vertical direction is reached, and the strength decrease linearly thereafter, as shown in Fig. 20. Bond strength is set as 0.5MPa referring to previous study (Chung *et al*. 2004), and the frictional coefficient at the joint boundary surface is set as 0.5 referring to preceding study (Korean Geotechnical Society 2009).

The load-displacement results from the experiment and analysis are compared in Fig. 21. The initial stiffness from analysis is slightly stiffer than the test results, but the overall structural behavior is similar. Table 4 compares the maximum load from the test and analysis results.

The tensile plastic strain distribution at the bottom of the specimen according to analysis results is shown in Fig. 22, and the plastic strain indicates crack occurrence in the specimen. The cracks develop from the loading surface to the center of the deck while relatively less cracks develop toward the lateral joint. The test and analysis results show similar crack behavior.

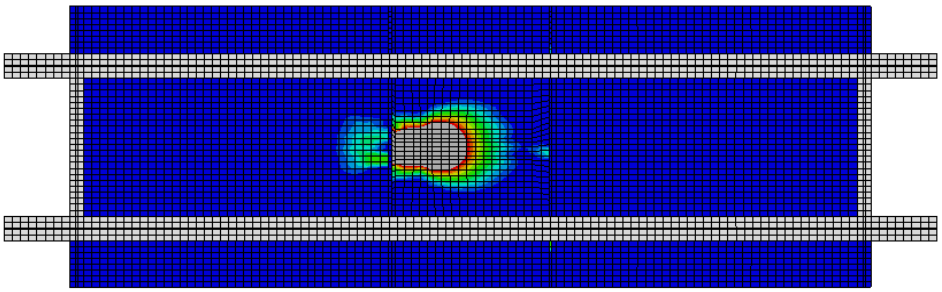

Fig. 22 Plastic strain distribution

Table 4 Comparison of the maximum load between experiment and analysis

Maximum Load(kN)		
Experiment	Analysis	Experiment/Analysis
1146.08	1077.68	1.06

6. Conclusions

In this study, an asymmetric precast deck system with ribbed loop joints is proposed. A composite bridge deck specimen is fabricated, and structural performance and serviceability of the proposed deck j system is evaluated through static and fatigue load tests. Leakage test of the deck joints and finite element analysis are also carried out. Conclusion is outlined as follows.

1) The proposed precast deck system is an asymmetric structure fabricated by assembling two types of prefabricated precast deck modules and pouring a filling material into the joint between the decks for integration. The proposed asymmetric precast deck system lack interference between the loop reinforcement and extended lower concrete at the joint, allowing sequential vertical installation and good workability. A separate form is not required at the site because the partition wall of the joint serves as a form when placing non-shrinkage mortar on the joint. Therefore, rapid construction is possible.
2) After completing the static load test applied with 200% of the deck design load, initial longitudinal cracks in the deck occur at the bottom of loading surface at a maximum load of 240kN by visual inspection, but lateral cracks do not occur.
3) After completing 2,000,000 cycles of the design fatigue load, the crack width of the joint is within the allowable crack width, and leakage in the joint between the decks and connections between the decks and steel girders do not occur. Moreover, after completing 100,000 cycles with three times the design fatigue load, stiffness of the deck is slightly reduced, but the deflection has a linear behavior. Thus, the serviceability is achieved with regard to crack and leakage under service load condition.
4) After applying static load until ultimate failure occur in deck, punching shear failure occur at maximum load of 1,146kN. The punching failure strength of the deck is approximately 9.1 times the design load considering impact effect.
5) Finite element analysis (FEA) show that structural behavior such as deflection and crack pattern of the precast deck is similar with test results, and FEA can be utilized effectively for verifying ultimate behaviors and parameter analysis study of precast deck system.

Acknowledgments

This study was supported by a grant (13SCIPA01) from Smart Civil Infrastructure Research Program funded by Ministry of Land, Infrastructure and Transport (MOLIT) of Korea government and Korea Agency for Infrastructure Technology Advancement (KAIA). The writer would like to acknowledge and thank MOLIT and KAIA for funding the study.

References

ABAQUS (2009), Abaqus Analysis User's Manual Version 6., 9, Dassault Systems Simulia Corp.
AASHTO (2008), LRFD Bridge Design Specification. 4th Ed., American Association of State Highway and Transportation Officials. Washington D.C., USA.
Chang, S.P., Kang, S.G. and Shim, C.S. (1997), "A study on the design of shear connector of continuous

composite bridge", *J. Korean Soc. Steel Constr.*, **9**(3), 351-362.
Chung, C.H., Lee, H.J., Hyun, B.H., Kim, J.S. and Park, K.M. (2004), *Evaluation and experiment of prefabricated PC manhole joint*, Research Report, Toam Industry Co., Ltd.
Chung, C.H., Shim, C.S., Kim, Y.J. and Jang, S.W. (1999), "Static and fatigue tests on composite bridge using precast concrete deck", *J. Korean Soc. Civil Engineers*, **34**(5), 791-800.
DAEWOO Corporation E&C (1998), Application and development of precast concrete bridge deck.
DIN 1045 (2001), Plain, reinforced and prestressed concrete structures.
Hognestad, E. (1951), "A study of combined bending and axial load in reinforced concrete members", *Bulletin 399*, University of Illinois Engineering Experiment Station, Urbana, III.
Issa, M.A., Idriss, A.T., Khayyat, S.Y. and Kaspar, I.I. (1995), "Full depth precast, prestressed concrete bridge decks panels", *PCI journal*, **39**(1), 59-80.
Issa, M.A., Issa, M.A., Idriss, A.T., Khayyat, S.Y., Yousif, A.A. and Kaspar, I.I. (1995), "Field performance of full depth precast concrete panels in bridge deck reconstruction", *PCI journal*, **40**(3), 82-108.
Joo, S.H., Chung, C.H. and Bae, J.H. (2014), "Strength evaluation on sectional members of prefabricated precast concrete arch with reinforced joint", *J. Korean Soc. Civil Engineers*, **34**(5), 1363-1372.
Kaushik, H.B., Rai, D.C. and Jain, S.K. (2007), "Stress-strain characteristics of clay brick masonry under uniaxial compression", *J. Mater. Civil Eng.*, **19**(9), 728-739.
Kim, I.G., Kim, Y.J., Kim, S.W. and Jang, S.K. (2007), "Rapid and mechanized construction of bridge deck with precast concrete deck system used longitudinal tendon", *J. Korea Concrete Inst.*, **19**(3), 50-54.
Kim, Y.J., Chung, C.H. and Park, C.L. (1997), "Application of precast concrete bridge decks for rapid construction", *J. Korea Concrete Inst.*, **9**(1), 68-75.
Kim, Y.J., Chung, C.H. and Shim, C.S. (1998), "A study on bond properties of joint grouting materials for precast concrete bridge decks", *J. Korea Concrete Inst.*, **10**(1), 153-160.
Kim, Y.J., Chung, C.H. and Shim, C.S. (2004), "New technology for durable concrete bridge decks", *J. Korea Concrete Inst.*, **16**(2), 10-16.
Korean Geotechnical Society (2009), Structure Foundation Design.
Ryu, H.K., Kim, Y.J. and Chang, S.P. (2007), "Experimental study on static and fatigue strength of loop joints", *Eng. Struct.*, **29**(2),145-162.
Shim, C.S., Choi, K.Y. and Chang, S.P. (2001), "Design of transverse joints in composite bridges with precast decks", *J. Korean Soc. Civil Engineers*, **5**(1), 17-27.
Shim, C.S., Lee, P.G., Jang, S.W. and Chang, S.P. (1999), "The Static and fatigue behavior of composite steel-concrete beam with precast concrete decks", *J. Korean Soc. Civil Engineers*, **19**(3), 417-425.
Shin, D.H., Park, S.J., Oh, H.C., Kim, I.G. and Kim, Y.J. (2015), "Evaluation on flexural performance of precast bridge decks with ribbed connection", *J. Korea Inst. Struct. Maint. Inspection*, **19**(3), 1-9.
Song, N.Y., Chung, C.H. and Kim, Y.J. (2009), "Nonlinear analysis of CFT truss girder with The arch-shaped lower chord", *J. Korean Soc. Civil Engineers*, **29**(6), 625-639.
Youn, S.K., Shim, C.S., Chung, C.H. and Chang, S.P. (1998), "Determination method for longitudinal prestressing force in precast bridge deck", *J. Korean Soc. Civil Engineers*, **18**(6), 799-810.